Water Science & Technology

IWA PUBLISHING

Water Science & Technology Vol 87 No 4, 834 doi: 10.2166/wst.2023.045

Experimental and DFT study of Cu(II) removed by Na-montmorillonite

Danqi Wang [a], Ruicong Wang[a], Wencai Peng[a,b,*], Jinli Zhang[c], Yi Wang[a], Minghui Huang[a], Na Zhang[a], Yanan Duan[a] and Ying Fang[a]

[a] School of Chemistry and Chemical Engineering, Shihezi University, Shihezi, Xinjiang 832003, China
[b] Key Laboratory for Green Processing of Chemical Engineering of Xinjiang Bingtuan, Shihezi, Xinjiang, China
[c] School of Chemical Engineering, Tianjin University, Tianjin 300350, China
*Corresponding author. E-mail: pengwencai@shzu.edu.cn

DW, 0000-0003-3351-9186

ABSTRACT

The experimental and theoretical studies on the adsorption of Cu(II) on the surface of Na-montmorillonite (Na-Mt) were reported. Effects of batch adsorption experimental parameters were studied. Density functional theory and molecular dynamics simulations were used to study the adsorption of Cu(II) on montmorillonite (001) surface. The adsorption reached equilibrium within 80 min and the adsorption capacity was 35.23 $mg{\cdot}g^{-1}$ at 25 °C. The adsorption data of Cu(II) were consistent with pseudo-second-order kinetics and Langmuir isotherm models. The adsorption process was dominated by physical adsorption (E_a was 37.08 $kJ{\cdot}mol^{-1}$) with spontaneous endothermic behavior. The influence of coexisting cations on the adsorption capacity of Cu(II) was Mg(II) > Co(II) > Ca(II) > Na(I). The simulation results demonstrated that there were no significant differences in the adsorption energy of Cu(II) at the four adsorption sites on the montmorillonite (001) surface. Cu(II) had more electron transfer than Na(I). The diffusion coefficient of Cu(II) in the aqueous solution system containing montmorillonite was $0.85{\times}10^{-10}$ $m^2{\cdot}s^{-1}$. Considerable amounts of Cu(II) ions were adsorbed at a distance of 0.26 and 2.25 Å from the montmorillonite (001) surface. The simulation results provided strong supporting evidence for experimental conclusions.

Key words: adsorption, Cu(II), molecular dynamics simulation, montmorillonite

HIGHLIGHTS

- The experimental and theoretical studies were used to study the mechanism of Cu(II) adsorption by Na-Mt.
- Adsorption of Cu(II) by Na-Mt was a monomolecular process and spontaneous process.
- Hirshfeld group analysis revealed a strong electrostatic attraction between Cu(II) and the surface of montmorillonite(001).
- The mechanism of adsorption of Cu(II) by Na-Mt was confirmed as ion exchange and electrostatic attraction.

GRAPHICAL ABSTRACT

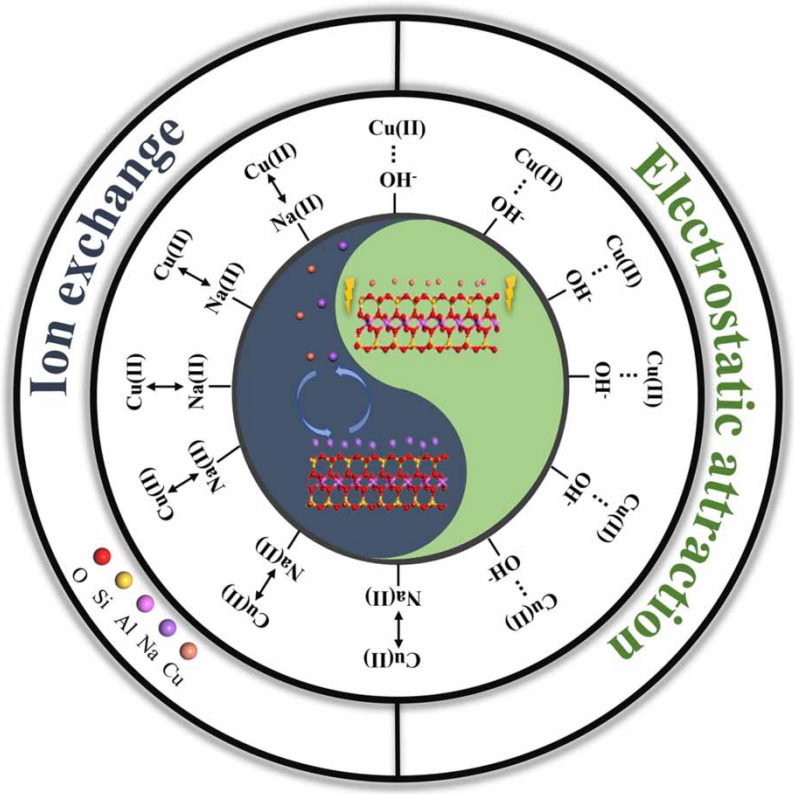

1. INTRODUCTION

In recent years, with the advancement of science and technology, the content of heavy metals (e.g. Cu(II), As(III), Pb(II) and Hg(I)) in the water environment has gradually increased, posing a serious threat to the stability of the Earth's ecosystem and the health of organisms (Turan & Ozgonenel 2013; Chen *et al.* 2015; Behera *et al.* 2021). Cu(II) in water mainly comes from industrial activities such as copper mining, brass manufacturing, electronics processing and non-ferrous metal smelting (Maskawat Marjub *et al.* 2019). The World Health Organization (WHO) recommends that the maximum quantity of Cu(II) in drinking water should be 0.2 $mg \cdot L^{-1}$, while the European Communities Directive sets it at 0.1 $mg \cdot L^{-1}$. Drinking excess copper-containing water (at a concentration greater than 6 $mg \cdot L^{-1}$) can cause vomiting, stomach cramps, skin irritation, nausea and anemia, while excess Cu(II) can be deposited in the kidneys, liver, brain and other human organs in enrichment, leading to Wilson's symptoms, hypertension, atherosclerosis and coronary heart disease, among many other adverse consequences (Paksamut & Boonsong 2018; Ameh & Sayes 2019; Pesavento *et al.* 2019; Chu *et al.* 2020). Therefore, the removal of Cu(II) is an important and urgent topic in heavy metal wastewater treatment technology.

The current methods for the removal of Cu(II) include ionic redox (de Carvalho *et al.* 2013), chemical precipitation (Fedje & Strömvall 2019), electrode-position (Schmidt *et al.* 2021), ion exchange (Antuganova *et al.* 2016; Groenendijk & van Wunnik 2021; Yousefzadeh *et al.* 2022), thermal deposition (Liu *et al.* 2018), biological methods (Szewczuk-Karpisz *et al.* 2021), liquid–liquid extraction (Molaei *et al.* 2018), membrane separation (Sharma *et al.* 2020), reverse osmosis (Abdullah *et al.* 2020; Hamid *et al.* 2020) and adsorption (Zhu *et al.* 2019; Giusto & Pissetti 2021; Xue *et al.* 2021). Among these methods, adsorption is efficient, simple, economical and widely used. Environmentally friendly and inexpensive adsorbent materials are a hotspot for current applications. Among them, montmorillonite has gained international attention as a potential adsorbent due to its large specific surface area, high cation exchange capacity, low-cost and no secondary environmental pollution (Zhu *et al.* 2019; Xue *et al.* 2021). Montmorillonite is a common clay mineral consisting of a 2:1 cationic layered mineral with aluminum octahedral sheets (Xiao *et al.* 2020). Isomorphic substitutions in the tetrahedral or octahedral sheet cause a negative charge on the montmorillonite lamellae that are neutralized by cations in the interlayer space. Hence, the

cationic interchangeability and electrostatic attraction of the montmorillonite are both important, which facilitates Cu(II) removal (Chen *et al.* 2015).

For the past few years, the adsorption performance of montmorillonite on Cu(II) has been studied by adsorption experiments. Zhou *et al.* (2012) investigated the adsorption performance of montmorillonite on a single heavy metal Cu(II) in simulated metallurgical wastewater, with a removal rate (RR) of 99.9% at a Cu(II) concentration of 50 $mg \cdot L^{-1}$. Turan & Ozgonenel (2013) investigated the removal efficiency of Cu(II) from industrial leachate by biosorption of montmorillonite and maximized the removal efficiency of Cu(II), achieving the optimization of the levels of the analyzed factors, resulting in a RR of 80.7% for Cu(II) with raw montmorillonite, which could be increased to 88.91% for the modified montmorillonite. Chen *et al.* (2015) used Na-Mt and Ca-Mt to remove Pb(II), Cu(II), Co(II), Cd(II), Zn(II) Ag(I), Hg(I) and Cr(VI) from aqueous solutions, finding that ion exchange was the main adsorption mechanism and Na-Mt was more effective for heavy metal adsorption than Ca-Mt and proved to be a potentially useful material for Pb(II), Cu(II), Co(II), Cd(II) and Zn(II) removal from aqueous solution. Atasoy & Bilgic (2017) studied the adsorption of Cu(II) by montmorillonite to explore the effectiveness of montmorillonite in environmental applications. The results showed that the adsorption of Cu(II) by montmorillonite reached 8.136 $mg \cdot g^{-1}$ by the Langmuir model. Montmorillonite feedstock had the potential to be used effectively in the production of low-cost adsorbents for the removal of copper from wastewater. Vezentsev *et al.* (2022) studied the adsorption of Cu(II) ions on bentonite (the main component is montmorillonite) as a function of the contact time and temperature of the medium. The adsorption of Cu(II) on bentonite clay increased as the temperature increased from 293 to 333 K. At the same time, the shape of the adsorption isotherms remains unchanged. Recently, adsorption experiments have been used to examine the characteristics of montmorillonite for the adsorption of Cu(II). However, the adsorption process is quite intricate that experimental approaches cannot fully explain the mechanism of Cu(II) adsorption. If the energy changes and kinetic parameters are investigated further from a quantum mechanical and molecular dynamics (MD) standpoint using molecular simulation techniques, insight into the microscopic mechanisms of Cu(II) adsorption on montmorillonite can be gained, allowing for a reasonable understanding and prediction of montmorillonite adsorption and modification. The density of states, electron transfer numbers, bonding locations and ionic ligand structures were investigated using density functional theory (DFT) and MD methods to fully understand the adsorption of heavy metal ions by minerals (Greathouse & Cygan 2005; Zhao & He 2014; Xing *et al.* 2015; Kong & Wang 2016). Therefore, it is still feasible to study the mechanism of Cu(II) adsorption by montmorillonite using a combination of experimental and simulation methods.

In this study, sodium-based montmorillonite (Na-Mt) was used as the adsorbent material and characterized by X-ray powder diffraction (XRD), Fourier transform infrared spectroscopy (FTIR), Brunner–Emmet–Teller (BET), scanning electron microscopy (SEM) and energy-dispersive spectroscopy (EDS). The adsorption of Cu(II) by Na-Mt in an aqueous solution was investigated under batch experimental conditions. The effects of adsorption time, initial Cu(II) concentration, temperature, initial pH, adsorbent dosage and coexisting cations on the adsorption effect were studied. In addition, cyclic regeneration experiments were carried out to investigate the locking ability of Na-Mt on heavy metal Cu(II). Finally, the $DMol^3$ module of Material Studio software based on the DFT was used to calculate the adsorption sites, energy changes and Hirshfeld population of montmorillonite. The Forcite module was applied to investigate the distribution characteristics, self-diffusion coefficients and concentration distribution of montmorillonite at the atomic level. The possible adsorption configuration and adsorption mechanism were given and analyzed.

2. MATERIALS AND METHODS

2.1. Materials

The sodium-based montmorillonite (Na-Mt) (PGW type) was produced from the Nanocor Company, USA. PGW, it has an ion exchange capacity of 145 mEq/100g, an aspect ratio of 200–400, a specific gravity of 2.6, a moisture content of 12% and an average particle size of 16–22 μm. For NVE, the microcanonical, or NVE, ensemble represents a system of a fixed number of particles (N), in a fixed volume (V), and with a fixed total energy (E). For NVT, application of classical Legendre transforms allows alternative ensembles to be derived, an example being the canonical, or NVT, ensemble, where a system can exchange heat with the environment and so remain at constant temperature (T). Copper chloride ($CuCl_2$) and cobalt chloride ($CoCl_2$) were purchased from Adamas-Beta. Magnesium chloride ($MgCl_2$) and calcium chloride ($CaCl_2$) were obtained from Macklin. Sodium nitrate ($NaNO_3$) and sodium chloride (NaCl) were purchased from the Shanghai Titan

Company. Hydrochloric acid (HCl) and sodium hydroxide (NaOH) were obtained from Tianjin Chemical Reagent Company. The reagents used in this study were all of the analytical grade and were not further purified.

2.2. Batch adsorption experiments

The effects of parameters including initial concentration, contact time, adsorbent dosage, initial pH, coexisting ions and reusability on Cu(II) adsorption were investigated in detail through batch adsorption experiments. The flowchart of the adsorption experiments is depicted in Figure 1. The adsorption experiments were carried out in a thermostat shaker at 200 rpm. Different parameters like initial concentrations (50–500 mg · L^{-1}), contact time (1–180 min), temperatures (25, 35 and 45 °C), adsorbent dosage (0.025–0.25 g), initial pH (3–8) and coexisting cations' (Mg(II), Co(II), Ca(II) and Na(I)) concentrations (10–150 mg · L^{-1}) were investigated. Unless otherwise stated, all relevant experiments were subjected to the following conditions: a solution volume of 50 mL and an adsorption time of 80 min. All solutions were centrifuged and the remaining Cu(II) concentration was detected using a Cu(II) selective electrode equipped with the MP523-01pH/ion concentration meter. The adsorption capacity (q_e) and RR are determined by Equations (1) and (2), respectively:

$$q_e = \frac{(C_0 - C_e)V}{m} \tag{1}$$

$$\mathrm{RR} = \frac{C_0 - C_e}{C_0} \times 100\% \tag{2}$$

where C_0 is the initial Cu(II) concentration (mg. L^{-1}) and C_e is the Cu(II) concentration (mg · L^{-1}) at equilibrium. V is the volume of the solution (L) and m is the amount of adsorbent used (Na-Mt) (g).

The adsorption data were analyzed using the Langmuir, Freundlich and Langmuir–Freundlich isotherms and could be represented in Equations (3)–(5), respectively (Tran *et al.* 2021):

$$q_e = \frac{Q_L K_L C_e}{1 + K_L C_e} \tag{3}$$

$$q_e = K_F C_e^{n_F} \tag{4}$$

$$q_e = \frac{Q_{LF}(K_{LF}C_e)^{n_{LF}}}{1 + (K_{LF}C_e)^{n_{LF}}} \tag{5}$$

where Q_L (mg · g^{-1}) is the Langmuir maximum adsorption capacity of the adsorbent (Na-Mt) and K_L (L · mg^{-1}) is the Langmuir equilibrium constant; K_F ($mg^{1-1/n}$ · ;$L^{-1/n}$ · g^{-1}) is the Freundlich constant and n_F (dimensionless) is the exponent of the Freundlich model; Q_{LF} (mg·g^{-1}) is the Langmuir–Freundlich maximum adsorption capacity of adsorbent (Na-Mt), K_{LF} (L · mg^{-1}) is the Langmuir–Freundlich equilibrium constant and n_{LF} (dimensionless) is the exponent of the Langmuir–Freundlich model.

Moreover, an essential dimensionless constant, R_L, referred to as the separation factor or equilibrium parameter, could be obtained from the Langmuir isotherm, which is used to predict the favorability of the adsorption process. The formula for R_L

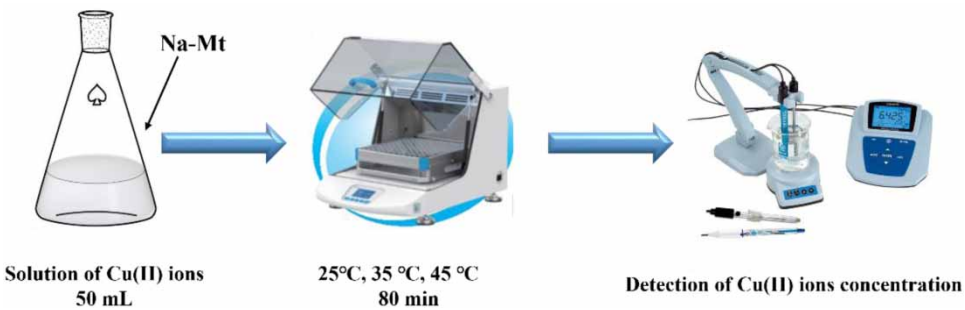

Figure 1 | Flowchart for adsorption experiments.

is given in Equation (6) (Chen *et al.* 2012):

$$R_L = \frac{1}{1 + K_L C_0} \tag{6}$$

The adsorption process is favorable when R_L is between 0 and 1 and unfavorable when $R_L > 1$. $R_L = 1$ means irreversible adsorption.

The change in standard free energy (ΔG^T), enthalpy (ΔH^T) and entropy (ΔS^T) of adsorption are calculated from Equations (7) and (8) (Lima *et al.* 2019; Tran 2022):

$$\Delta G^T = -RT \ln K_{Eq}^{\circ} \tag{7}$$

$$\ln K_{Eq}^{\circ} = \frac{\Delta S^T}{R} - \frac{\Delta H^T}{RT} \tag{8}$$

where R is the ideal gas constant ($8.314\ \mathrm{J \cdot mol^{-1} \cdot K^{-1}}$) and T is the adsorption temperature (K).

The equilibrium constant (K) of the adsorption isotherm model is converted to a dimensionless K_{Eq}° and applied to the thermodynamic parameters as shown in Equation (9) (Lima *et al.* 2019; Tran *et al.* 2021):

$$K_{Eq}^{\circ} = K \times 1,000 \times M_w \times \frac{C_{Adsorbate}^{\circ}}{\gamma_{Adsorbate}} \tag{9}$$

where K represents the equilibrium constant of the adsorption isotherm model, M_w ($\mathrm{g \cdot mol^{-1}}$) is the molar weight of adsorbate ($M_{Cu} = 64\ \mathrm{g \cdot mol^{-1}}$), $C_{Adsorbate}^{\circ}$ is the standard concentration of adsorbate ($1\ \mathrm{mol \cdot L^{-1}}$), and $\gamma_{Adsorbate}$ (dimensionless) is the activity coefficient of adsorbate, which is equal to 1.

To accurately reflect the rate of mass transfer in the adsorption process and desorption rate, as well as the adsorption mechanism, pseudo-first-order, pseudo-second-order, intraparticle diffusion and Elovich kinetic equations are used to interpret the experimental data. Equations (10)–(13) of the four models are as follows (Azizian 2004; Douven *et al.* 2015):

$$q_t = q_e(1 - e^{-K_1 t}) \tag{10}$$

$$q_t = \frac{K_2 q_e^2 t}{1 + K_2 q_e t} \tag{11}$$

$$q_t = K_3 t^{0.5} + C \tag{12}$$

$$q_t = \frac{1}{\beta} \ln(\alpha\beta) + \frac{1}{\beta} \ln t \tag{13}$$

where q_t ($\mathrm{mg \cdot g^{-1}}$) is the adsorbed capacity of Cu(II) adsorbed per unit Na-Mt at time t and K_1, K_2, K_3 and C are all kinetic equation constants. If $C = 0$, it is indicative of an adsorption process only controlled by the intraparticle diffusion mechanism. The parameter α ($\mathrm{mg \cdot g^{-1} \cdot min^{-1}}$) is defined as the initial adsorption rate and β ($\mathrm{g \cdot mg^{-1}}$) is the desorption constant of this process.

The activation energy (E_a) reflects whether the adsorption process of the adsorbent with the metal ions is physical or chemical adsorption. The value of the activation energy is calculated from the Arrhenius equation, as seen in Equation (14) (Tseng *et al.* 2022):

$$k_0 = A e^{-\left(\frac{E_a}{RT}\right)} \tag{14}$$

where k_0 is the rate constant, A is the Arrhenius constant and E_a is the activation energy.

2.3. Desorption and reusability

Five adsorption–desorption experiments were performed to evaluate the recoverability of the Na-Mt material. For each adsorption–desorption cycle, the dosage of Na-Mt ($2\,g \cdot L^{-1}$) and the initial concentration of Cu(II) ($100\,mg \cdot L^{-1}$) were kept constant and the contact time was 80 min, then the used Na-Mt material was immersed in 1 M NaCl solution. After each adsorption–desorption cycle, the Na-Mt material was filtrated, washed with deionized water and dried at 105 °C for the next adsorption.

2.4. Simulation method and process

The simulations ($DMol^3$ and Forcite modules) were completed using Materials Studio software. The DFT calculation was implemented in the $DMol^3$ program using the generalized gradient approximation (GGA) with the Perdew-Burke-Ernzerhof (PBE) functional (Perdew *et al.* 1996). A Grimme dispersion correction was added to the DFT calculation (Grimme 2006). In addition, spin unrestricted and formal spin as initial were also used in all calculations of the $DMol^3$ module. The basic set of atomic orbitals used in the calculation was double numerical plus polarization (DNP). The core electrons were treated with effective core potentials (ECP), which provide no special treatment of cores. The number of integration points that used to integrate the wavefunction in reciprocal space was $3 \times 2 \times 1$ (Kong & Wang 2016). The self-consistent field (SCF) convergence was set to 1×10^{-6} eV per atom. The effect of water on the adsorption was studied with the aid of the conductor-like screening model (COSMO) as implemented in $DMol^3$ program, where the solvent was treated as a dielectric continuum. Based on the above settings, the configuration optimization and related energy (ΔE_{ads}) calculation of the montmorillonite unit cell model established were performed. In addition, the Hirshfeld population was analyzed by means of an optimized Cu(II) with montmorillonite model and a Na(I) with montmorillonite model.

In this study, the initial structure of montmorillonite was modeled by referring to literature (Viani *et al.* 2002). The parameters of the unit cell were $a = 5.180$ Å, $b = 8.980$ Å, $c = 15.000$ Å, $\alpha = \beta = \gamma = 90°$. The cleavage of the (001) crystal plane was performed on the montmorillonite unit cell and a vacuum of 15 Å was added on the surface along the *c*-axis to minimize the artificial interference from the adjacent layer. Moreover, the charged nature of the montmorillonite laminate endowed its surface model with a negative charge and all the DFT and MD calculations for adsorption were executed on this plane.

Considering that Cu(II) or Na(I) may have different adsorption sites on the (001) crystal face of montmorillonite, we investigated the adsorption sites of Cu(II) or Na(I) through the Top, Bridge and Hollow sites. The adsorption energies between Cu(II) or Na(I) and montmorillonite laminate at different adsorption sites (Top, Bridge and Hollow sites) were also studied. The calculation formula for the adsorption energy (ΔE_{ads}) of the Cu(II) or Na(I) and montmorillonite laminate is shown in Equation (15):

$$\Delta E_{ads} = E_{M-Mt} - (E_{Mt} + E_M) \tag{15}$$

where ΔE_{ads} is the adsorption energy of Cu(II) or Na(I) and montmorillonite laminate, E_{M-Mt} is the total energy of Cu(II) or Na(I) adsorption configuration on the montmorillonite laminate, E_{Mt} is the energy of the montmorillonite laminate, E_M is the energy of Cu(II) or Na(I) and their units are all $kJ \cdot mol^{-1}$.

MD involves the stepwise integration of Newton's equations from a given starting point. It is the most natural method of performing equilibrium statistical-mechanical calculations through a simulation. MD simulation calculations were executed with periodic periphery conditions in three dimensions. The supercell model of montmorillonite $4a \times 2b \times 1c$ was constructed on the basis of the unit cell, with *x*- and *y*-axis lengths of 20.72 and 17.96 Å, respectively (Peng *et al.* 2018; Chu *et al.* 2019; Zhu *et al.* 2019). This provided an appropriate montmorillonite surface for MD studies of Cu(II) adsorption. In order to obtain a realistic model of a clay mineral in contact with an aqueous solution, 480 water molecules and 20 Cu(II) were added to the interlayer of montmorillonite supercell during the simulation process. Firstly, the structure of the completed simulation box was optimized and annealed using the Forcite module and then the MD simulation was performed. Anneal algorithm for structural relaxation was used in microcanonical ensemble synthesis (NVE) with an equilibrium time of 500 ps (Zhu *et al.* 2019). For NVE, the microcanonical, or NVE, ensemble represents a system of a fixed number of particles (N), in a fixed volume (V), and with a fixed total energy (E). The final balanced structures of the NVE ensemble simulations were regarded as the initial structures of the canonical (NVT) ensemble simulations (Zhu *et al.* 2019). For NVT, application of classical Legendre transforms allows alternative ensembles to be derived, an example being the canonical, or NVT, ensemble, where a system can exchange heat with the environment and so remain at constant temperature (T). All the dynamic time step

was 1 fs, the NVT simulation time was 1,000 ps and the number of dynamic steps was 1×10^6. UFF (Universal force field) was applied and the Ewald method and the atom-based method were used to calculate the long-range electrostatic interaction and the van der Waals interaction, respectively (Zhu *et al.* 2019). The experiments ($T = 298$ K, 1×10^5 Pa) were carried out using a Nose thermostat with the pressure regulated by a Berendsen constant pressure device and all atoms were relaxed (Zhu *et al.* 2019). In addition to the MD simulation of Cu(II) in an aqueous solution in the presence of montmorillonite, the kinetic behavior of Cu(II) in an aqueous solution was simulated and analyzed. The concentration distribution of Cu(II) adsorbed by montmorillonite was analyzed. Then, the mean square displacement (MSD) curve was drawn and the diffusion coefficient of Cu(II) was calculated. Finally, the radial distribution function of Cu(II) adsorption on montmorillonite was analyzed.

3. RESULTS AND DISCUSSION

3.1. Characterization

SEM analysis is widely used to investigate the surface morphology of materials. Figure 2 shows SEM and EDS images of Na-Mt before and after adsorption (Cu-Mt). Both Na-Mt and Cu-Mt exhibit stacked lamellar structures at the 1 μm scale and at the smaller 400 nm scale and it is clearer that both have irregular sheet-like structures. This indicates that the structure of Cu-Mt has not changed. As can be seen in Figure 2(a3) and 2(b3), it was found that after adsorption, the peak of Na disappeared (from 2.41 to 0 wt%) and the peak of Cu appeared (from 0 to 3.95 wt%). This suggests that ion exchange occurs between Cu(II) and Na(I) in the montmorillonite.

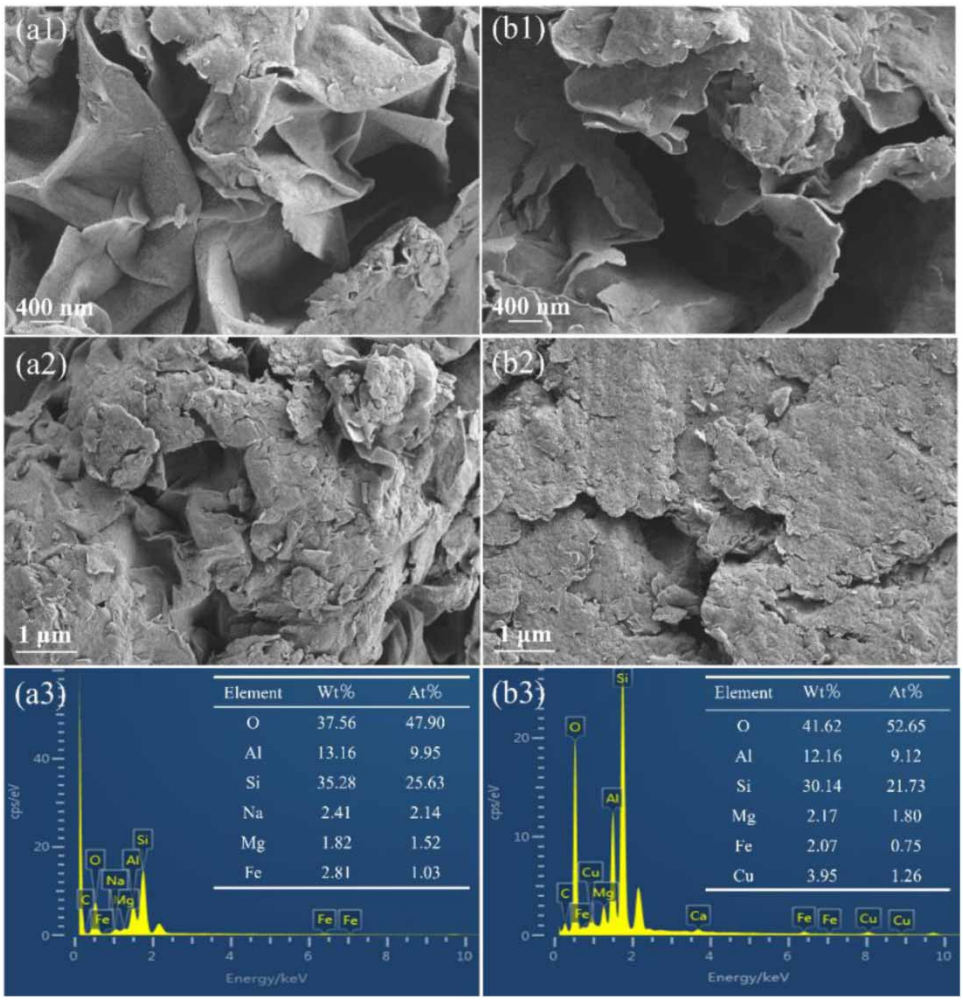

Figure 2 | SEM images of Na-Mt (a1 and a2) and Cu-Mt (b1 and b2) with EDS spectra of Na-Mt (a3) and Cu-Mt (b3).

XRD is a research method for analyzing the crystal structure of materials. Figure 3 presents the XRD patterns of the Na-Mt, Cu-Mt and $Al_2(Si,Al)_4O_{10}(OH)_2{\cdot}2H_2O$ (PDF#43-0688). The peaks appearing around 7.213° (001), 19.801° (100), 28.775° (004) and 34.882° (110) fit the standard card (PDF#43-0688) well, which corresponds to the montmorillonite crystal structure. Comparing the (001) peaks for both Na-Mt and Cu-Mt, the diffraction angle of Cu-Mt is smaller (6.897°) than that of Na-Mt (7.123°). Accordingly, the d_{001} value after adsorption (Cu-Mt) increased from the original (Na-Mt) 1.24 to 1.28 nm. It further shows that ion exchange interaction of Cu(II) ions with Na(I) ions in montmorillonite (Liu *et al.* 2021). The high XRD similarities between the two suggest that the adsorption process did not destroy the layered skeletal structure of Na-Mt.

FTIR spectra of Na-Mt and Cu-Mt are detected in the range of 4,000–500 cm^{-1} of wavenumber. In Figure 4, the band near 3,627 cm^{-1} is ascribed to the stretching vibration bands of hydroxyl groups (–OH) on Na-Mt octahedral laminates. The bending vibration bands around 1,643 and 1,037 cm^{-1} are associated with H–O–H and Si–O–Si. The stretching vibration bands around 915, 522 and 465 cm^{-1} are related to Al–O–(OH)–Al, Si–O–Al and Al–OH.

The isotherms of N_2 adsorption–desorption for Na-Mt and Cu-Mt samples are displayed in Figure 5 and the corresponding specific area, average pore width and pore volume are listed in Table 1. It can be seen that the two curves are similar with each other, which also means that the adsorption of Cu(II) by Na-Mt does not have a significant effect on the material properties. The isotherms correspond to Type-IV and the hysteresis loops conform to Type-H3, according to the IUPAC classification, indicating that they are mesoporous materials. Moreover, the specific surface area increased from 7.054 to

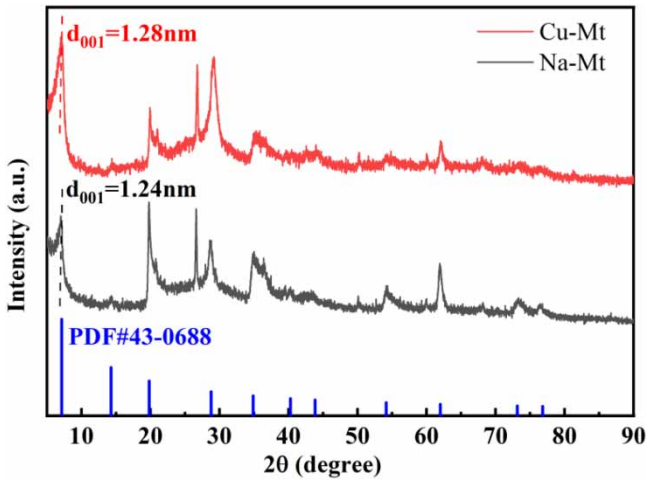

Figure 3 | The XRD patterns of Na-Mt, Cu-Mt and PDF#43-0688.

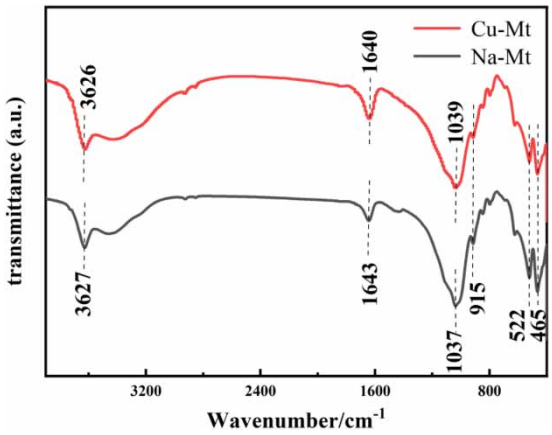

Figure 4 | The FTIR spectra of Na-Mt and Cu-Mt.

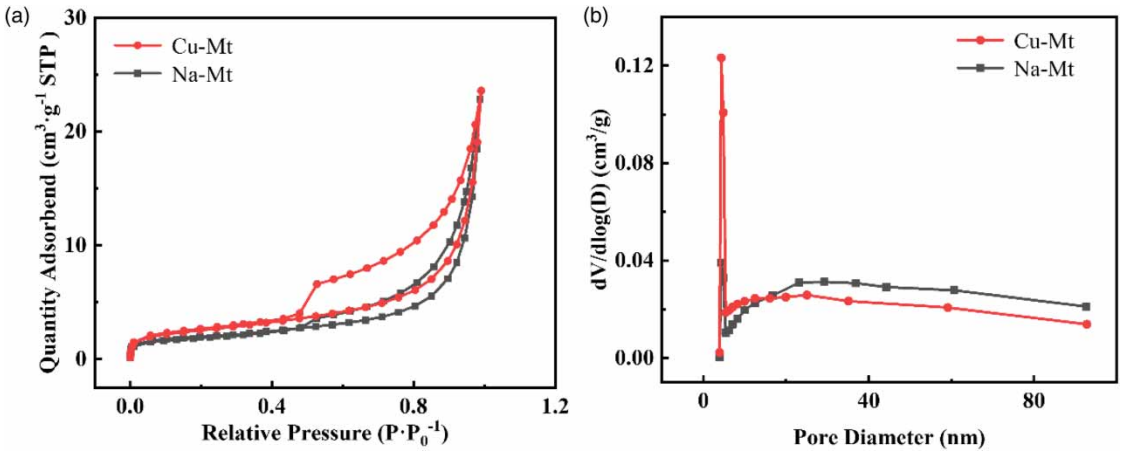

Figure 5 | Nitrogen adsorption and desorption isotherms of Na-Mt and Cu-Mt (a) and pore size distributions of Na-Mt and Cu-Mt (b).

Table 1 | The textural properties of Na-Mt and Cu-Mt

Sample	S_{BET} ($m^2 \cdot g^{-1}$)	Da (nm)	V_t ($cm^3 \cdot g^{-1}$)
Na-Mt	7.054	10.004	0.018
Cu-Mt	9.006	8.836	0.020

9.006 $m^2 \cdot g^{-1}$, the pore volume increased from 0.018 to 0.020 $cm^3 \cdot g^{-1}$ and the pore size decreased from 10.004 to 8.836 nm for Cu-Mt compared with Na-Mt. This may be due to the repulsion of the adsorbed Cu(II) from each other, resulting in a lower density of accumulation between them and thus exhibiting a higher specific surface area.

3.2. Adsorption studies

3.2.1. Effect of contact time on the adsorption of Cu(II)

The effect of contact time on the adsorption of Cu(II) by Na-Mt at three temperature conditions (25, 35 and 45 °C) is shown in Figure 6(a). The equilibrium adsorption capacity of Cu(II) increased with the increase in contact time (0–30 min) and the equilibrium adsorption capacity of Cu(II) tended to be constant at 35.23 $mg \cdot g^{-1}$ after 80 min. This is attributed to the rapid adsorption of Cu(II) at the initial stage of the adsorption process resulting from the abundance of active sites in the adsorbent and the high concentration difference between the solid and liquid phases. As adsorption proceeds, the concentration of Cu(II) in solution decreases and most of the active sites on the adsorbent surface are occupied, contributing to a weaker driving force for mass transfer between the adsorbent and the adsorbate, thus reducing the rate of adsorption and diffusion of Cu(II). The experimental data were fitted and analyzed using pseudo-first-order, pseudo-second-order, intraparticle diffusion and Elovich kinetic models (Equations (10)–(13) and the results are shown in Figure 6(b)–6(e) and Table 2. The correlation coefficient (R^2) calculated from the pseudo-second-order kinetic model ($R^2 = 0.942$ at 25 °C) was greater than that of pseudo-first-order kinetic model, the intraparticle diffusion model ($R^2 = 0.576$ at 25 °C) and the Elovich model ($R^2 = 0.863$ at 25 °C). The equilibrium adsorption capacity (34.98 $mg \cdot g^{-1}$ at 25 °C) calculated by the pseudo-second-order model was similar to the actual adsorption capacity (35.23 $mg \cdot g^{-1}$ at 25 °C), indicating that pseudo-second-order kinetic equation could better fit the adsorption of Cu(II) by Na-Mt. In addition, the adsorption capacity of the Na-Mt was highest at $T = 45$ °C and the lowest at $T = 25$ °C, indicating that high temperature was beneficial for the adsorption of Cu(II).

3.2.2. Activation energy

Based on the results of the analysis of the adsorption kinetics in Section 3.2.1, the value of the activation energy E_a can be + derived by selecting the natural logarithm of the rate constant of the pseudo-second-order kinetic equation to plot against $1/T$, as depicted in Supplementary Figure S1 (Chen *et al.* 2021b; Tseng *et al.* 2022). The adsorption activation energy (E_a) was calculated to be 37.08 $kJ \cdot mol^{-1}$. It was reported that an E_a of 40 $kJ \cdot mol^{-1}$ was the critical value to distinguish physical

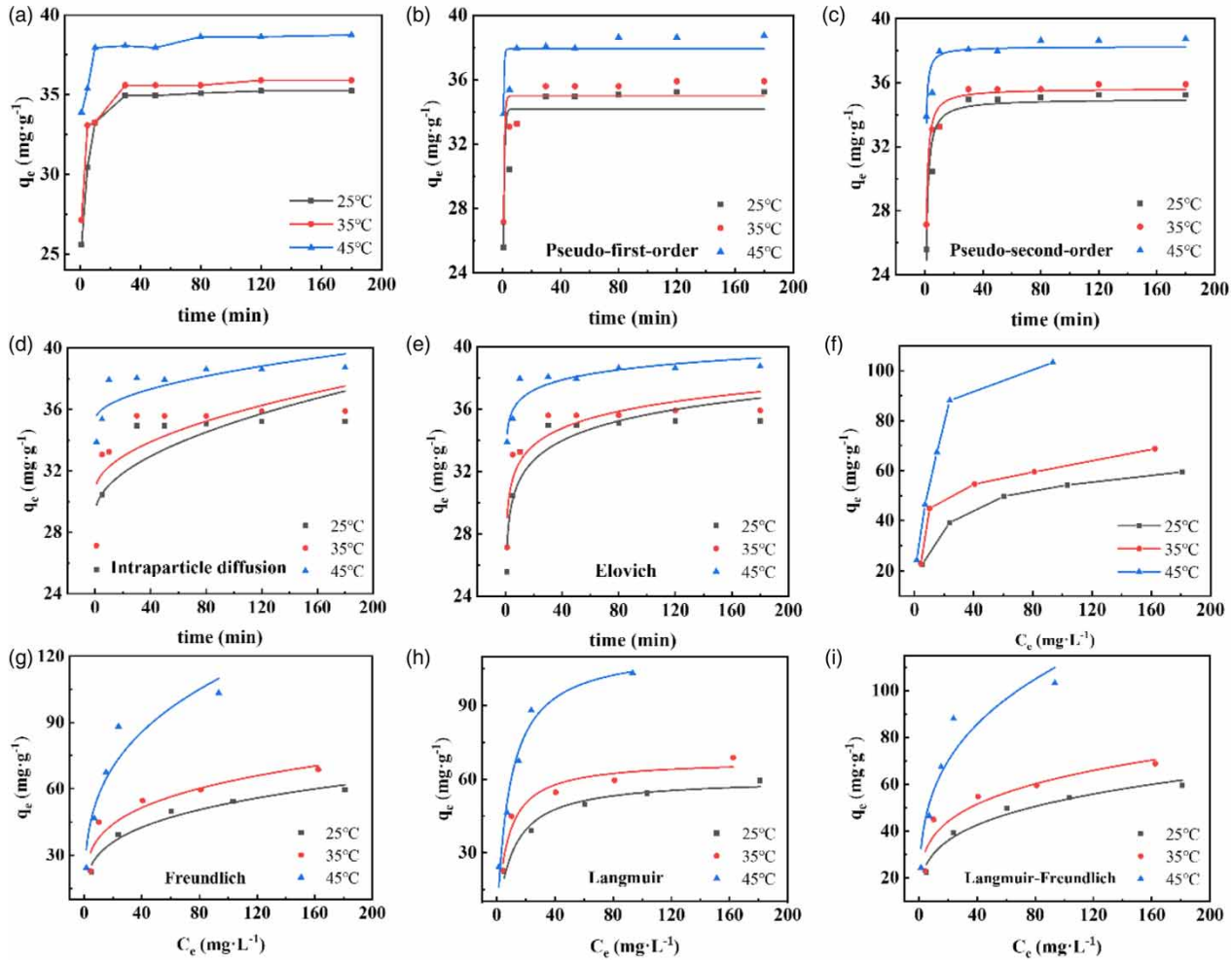

Figure 6 | Effect of contact time on the adsorption of Cu(II) by Na-Mt at the three temperatures (a), and kinetic models simulated plots for the adsorption of Cu(II) by Na-Mt (b–e); effect of the initial Cu(II) concentration on the adsorption of Cu(II) by Na-Mt at three temperatures (f) and thermodynamic models simulated plots for the adsorption of Cu(II) by Na-Mt (g–i).

adsorption (<40 kJ · mol^{-1}) and chemical adsorption (>40 kJ · mol^{-1}), thus the adsorption process of Cu(II) by Na-Mt was dominated by physical adsorption (Chen *et al.* 2021a).

3.2.3. Effect of initial concentration on the adsorption of Cu(II)

The effect of the initial Cu(II) concentration on the adsorption of Cu(II) by Na-Mt at three temperature conditions (25, 35 and 45 °C) is presented in Figure 6(f). It can be noticed that as the equilibrium concentration of Cu(II) increased, the equilibrium adsorption capacity exhibited a trend of steep increase first followed by a gentle increase. To figure out the relationship between the adsorbent and the adsorbate, adsorption isotherm models, including the Langmuir model, Freundlich model and Langmuir–Freundlich model (Equations (3)–(5) were used for modeling these adsorption isotherm data. The fitting results are shown in Figure 6 –6(i) and the relevant parameters are listed in Table 3. The correlation coefficient (R^2) of the Langmuir isotherm model ($R^2 = 0.974$ at 25 °C) was greater than that of the Freundlich isotherm model ($R^2 = 0.969$ at 25 °C) and Langmuir–Freundlich model ($R^2 = 0.969$ at 25 °C). From the result, the Langmuir isotherm model can fit the adsorption process of Cu(II) by Na-Mt, reflecting that the adsorption process of Cu(II) by Na-Mt is mainly monolayer adsorption. The Q_L values fitted to the Langmuir equation showed an increase from 60.32 to 113.75 mg · g^{-1} with increasing temperature, illustrating the significant effect of raising the temperature on the adsorption process. The separation factor R_L was 0–1 in the range of 25–45 °C, suggesting that the adsorption process is favorable at all three temperatures.

Table 2 | Kinetics parameters for the adsorption of Cu(II) by Na-Mt at 25–45 °C

Model	25 °C	35 °C	45 °C
Pseudo-first-order			
q_e	34.17	34.99	37.90
K_1	1.37	1.49	2.24
R^2	0.776	0.852	0.633
Pseudo-second-order			
q_e	34.98	35.63	38.25
K_2	0.07	0.09	0.18
R^2	0.942	0.965	0.811
Intraparticle diffusion			
C	29.18	30.66	35.29
K_3	0.60	0.51	0.32
R^2	0.576	0.558	0.630
Elovich			
α	6.37×10^6	1.97×10^8	9.22×10^{15}
β	0.55	0.64	1.07
R^2	0.863	0.841	0.862

Table 3 | Parameters related to the adsorption isotherm of Cu(II) by Na-Mt at 25–45 °C

Model	25 °C	35 °C	45 °C
Langmuir			
Q_L	60.32	67.80	113.75
K_L	0.09	0.14	0.11
R_L	0.03 ~ 0.18	0.02 ~ 0.12	0.03 ~ 0.15
R^2	0.974	0.948	0.968
Freundlich			
K_F	17.12	22.41	29.04
n	4.05	4.44	3.41
R^2	0.969	0.892	0.911
Langmuir–Freundlich			
Q_{LF}	35.68	41.57	101.70
K_{LF}	0.05	0.06	0.01
n	0.25	0.23	0.29
R^2	0.969	0.892	0.911

3.2.4. Thermodynamic parameter analysis

The thermodynamic parameters ΔG^T, ΔH^T and ΔS^T (Equations (7)–(9) are investigated to analyze the driving forces of adsorption or to determine whether the adsorption process is spontaneous. As shown in Supplementary Figure S2, ΔH^T and ΔS^T were obtained from the slope and intercept of van't Hoff plots of $\ln K^{\circ}_{Eq}$ vs. $1/T$. The thermodynamic parameters for the adsorption are listed in Table 4. The ΔH^T and ΔS^T values were positive at three temperature conditions (25, 35 and 45 °C), indicating that the adsorption of Cu(II) by Na-Mt was an endothermic and entropy-increasing process. The values of ΔG^T

Table 4 | Thermodynamic parameters for the adsorption of Cu(II) by Na-Mt

T (°C)	ΔG^T (kJ · mol^{-1})	ΔH^T (kJ · mol^{-1})	ΔS^T (J mol^{-1} · K^{-1})
25	−21.6	6.9	95.6
35	−22.6		
45	−23.5		

were negative at three temperature conditions (25, 35 and 45 °C), implying that the adsorption process of Cu(II) by Na-Mt was a spontaneous process. And the absolute values of ΔG^T increased with increasing temperature, indicating that increasing the temperature is beneficial for the adsorption to proceed to the right, thus the adsorption capacity of Na-Mt on Cu(II) is increased. Furthermore, the removal of Cu(II) from aqueous solutions by Na-Mt is not a simple adsorption process, but also affected by solvent effect and ion exchange, which cause a different phenomenon from that shown by normal adsorption processes ($\Delta H < 0$ and $\Delta S < 0$).

A universal trend is that hydration strongly depends on the radius of the ion, with the smaller ions being better solvated. From the Bron Equation (16), it follows that the divalent ion has roughly quadrupled the hydration energy that of the monovalent ion. Consistent with this electrostatic analysis, divalent cations have much larger hydration energies than monovalent cations. This is also consistent with previously reported conclusions (Unuabonah *et al.* 2016; Adapa & Malani 2018), where the hydration energy of Na(I) was −87.24 kcal · mol^{-1}, while that of Cu(II) was 507.00 kcal · mol^{-1}. Thus, Cu(II) has a larger charge and smaller radius than Na(I), so the hydration energy of Cu(II) is greater than that of Na(I), suggesting that Cu(II) can bind more water molecules than Na(I), forming hydrated copper ions and also that the H_2O surrounding Cu(II) is partially liberated as free water molecules during ion exchange adsorption, which may contribute to the increase in entropy:

$$E_{\text{sol}} = -(1 - 1/\varepsilon)(q^2/8\pi\varepsilon_0 a) \tag{16}$$

where ε is the dielectric constant of the solvent (for water, $\varepsilon = 78$), a is the radius of the ion (for Na(I), $a = 1.02$ Å; for Cu(II), $a = 0.73$ Å) and q is the charge of the ion (for Na(I), $q = 1$; for Cu(II), $q = 2$).

3.2.5. Effect of adsorbent dosage on the adsorption of Cu(II)

Figure 7(a) shows the effect of the dosage of Na-Mt material on the adsorption of Cu(II). With the increase of Na-Mt dosage, the adsorption capacity of Cu(II) decreased from 61.81 to 19.97 mg · g^{-1}. When the adsorbent increased from 0.1 to 0.15 g, the upward trend in RR became gentler and the RR was close to 96%. This may be due to the fact that at lower dosing levels, the exposed adsorption sites are heavily occupied by Cu(II) ions. When the adsorbent dosage is increased, the Cu(II) concentration gradient is smaller in the later stage of adsorption process, resulting in weaker Cu(II) ions adsorption.

3.2.6. Effect of coexisting cations on the adsorption of Cu(II)

In practice, Cu(II) is not the only cation present in water, so four cations (Na(I), Ca(II), Co(II) and Mg(II)) were selected as representatives to study the effect of coexisting cations on the adsorption capacity of Cu(II). The effect of different cations on the adsorption capacity of Cu(II) with different concentrations are shown in Figure 7(b). The adsorption capacity of Cu(II) by Na-Mt decreased as the concentration of coexisting cations increased. The order of influence on the adsorption capacity of Cu(II) by Na-Mt was Mg(II) > Co(II) > Ca(II) > Na(I). This is because in ion exchange, the higher the valence of the ion and the smaller the radius, the more likely the ion exchange will occur. If the adsorption process of montmorillonite materials follows the electrostatic principle, the higher the value of Z/r (charge/radius) the greater the affinity, then the affinity of the multivalent ion is greater than that of the monovalent ion (Ucarli *et al.* 2020). The magnitude of Z/r is Mg(II) (2/72) > Co(II) (2/74.5) > Ca(II) (2/100) > Na(I) (1/102) (Marcus 1993), which corresponds to the order in the diagram.

3.2.7. Effect of initial pH on the adsorption of Cu(II)

The effect of pH on the adsorbent is a significant factor in adsorption experiments. Therefore, the adsorption capacity of Cu(II) at pH 3–8 was studied. The effect of pH on adsorption was investigated by adjusting the initial pH with 0.1 M NaOH solution and 0.1 M HCl solution. The adsorption result is shown in Figure 7(c) and the adsorption capacity of Cu(II) gradually increased from 21.22 (pH = 3) to 49.80 mg · g^{-1} (pH = 8) with increasing pH. When the pH in the solution

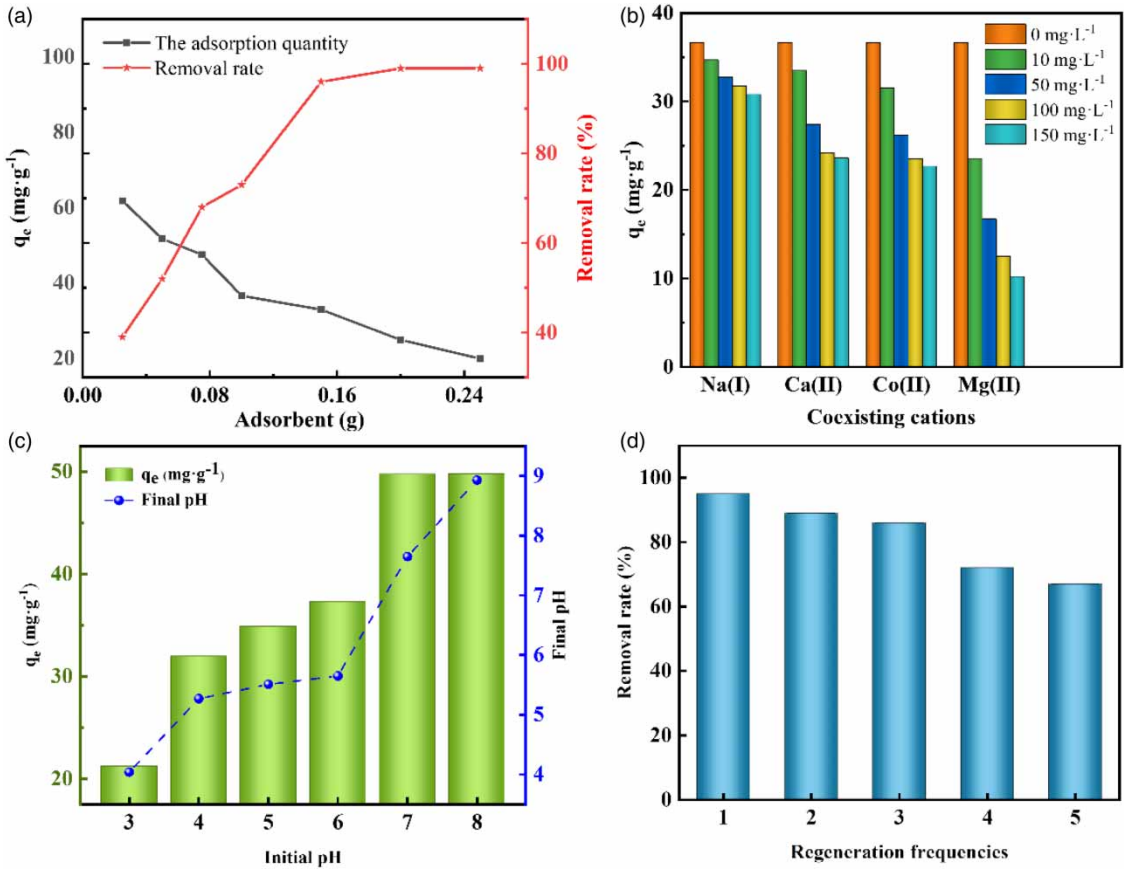

Figure 7 | Effect of adsorbent dosage on the adsorption of Cu(II) (a), and effect of coexisting ions with different concentrations on adsorption of Cu(II) (b), and effect of initial pH on the adsorption of Cu(II) (c) and the reusability for Cu(II) by Na-Mt (d).

is low, a large amount of H^+ is present in the solution and the H^+ and Cu(II) ions will compete with each other for the adsorption sites on Na-Mt. A part of the H^+ will occupy the adsorption sites on Na-Mt, weakening the adsorption of Cu(II); when the pH in the solution is further increased, the presence of a large amount of OH^- in the solution makes it easy for Cu(II) to precipitate $Cu(OH)_2$ or $Cu(OH)^+$ complexes on the Na-Mt surface, resulting in an increase in adsorption capacity. This is also in agreement with the trend of similar previous studies (Han *et al.* 2018).

3.3. Desorption and reusability

In practical applications, the adsorbent can be used repeatedly for the purpose of reusing to save material, which is the key to economic attractiveness, so we tested the recycled performance of the adsorbed Na-Mt. The reusability experiments of Cu(II) by Na-Mt were carried out and five adsorption–desorption cycles were repeated, as depicted in Figure 7(d). The results showed that the removal efficiency of Cu(II) decreases from 95 to 67% with increasing times of the reuse after five cycles. This indicated that Na-Mt adsorbent is quite stable and feasible for the repeated application of heavy metals such as Cu(II).

3.4. Molecular simulation for adsorption process

3.4.1. Adsorption site and adsorption energy

There were four possible adsorption sites as shown in Figure 8, which were Bridge site (1), Hollow site (2), Top of O_1 site (3) and Top of O_2 site (4). The adsorption energies of Na(I) or Cu(II) of four adsorption sites on the (001) crystal face of montmorillonite are calculated by Equation (15), as shown in Supplementary Table S1. The adsorption energies of Na(I) at the Bridge site, Hollow site, Top of O_1 site and Top of O_2 site were −1,118.89, −1,040.07, −1,005.33 and −924.91 kJ · mol^{-1}, respectively. Similarly, the adsorption energies of Cu(II) at the Bridge site, Hollow site, Top of O_1 site and Top of O_2 site were −2,112.50, −2,065.88, −2,072.84 and −2,277.49 kJ mol^{-1}, respectively. The results demonstrate that the adsorption

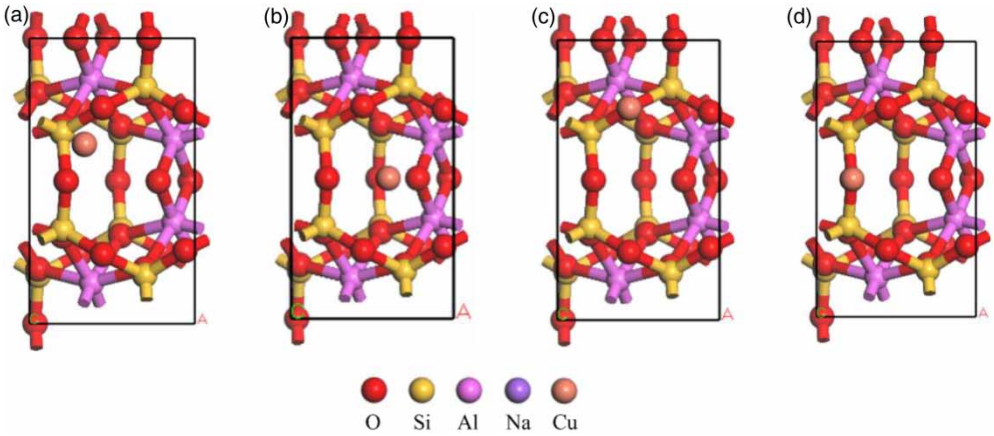

Figure 8 | Optimized adsorption configurations of Cu(II) adsorption at different adsorption sites Bridge site (a); Hollow site (b); Top of O_1 site (c) and Top of O_2 site (d).

energies of Na(I) at the four adsorption sites were not remarkably different, as was the case for Cu(II), which was in accordance with Langmuir's hypothetical conditions. Moreover, the adsorption of Cu(II) at all four sites was more stable than that of Na(I), so that Cu(II) in an aqueous solution was adsorbed onto the montmorillonite by ion exchange adsorption with Na(I) between the montmorillonite layers. This is also consistent with the results of XRD and SEM-EDS characterization of the adsorption mechanism.

3.4.2. Hirshfeld population analysis

The adsorption of Na(I) or Cu(II) on montmorillonite are mainly an electrostatic attraction and this interaction can lead to the transfer of electrons between the interlayer cations and the laminate. By analyzing the Hirshfeld charges of Al, Si, O and interlayer cations in montmorillonite before and after adsorption, the charge transfer that occurred when the montmorillonite interacted with cations was verified. Therefore, Hirshfeld population analysis was used to calculate the charges of the atoms after adsorption on montmorillonite and the results are shown in Supplementary Table S2. It was found that the charge transfer amount of Cu(II) was more than that of Na(I), indicating that the electrostatic attraction between Cu(II) and montmorillonite laminate may be stronger than the electrostatic attraction between Na(I) and montmorillonite laminate. This is consistent with the conclusion that the interaction between Cu(II) and the laminate is stronger for adsorption energy studies.

3.4.3. Concentration profiles of montmorillonite before and after adsorption

Figure 9(a) and 9(b) displays the final equilibrium conformation of the Cu(II) distribution in pure aqueous solution and after adsorption of Cu(II) by montmorillonite(001). It can be clearly seen that a large amount of Cu(II) in the skeleton after the addition of the montmorillonite model was adsorbed on the surface of the montmorillonite by electrostatic attraction. This is also consistent with the experimental data and SEM-EDS results. Supplementary Figure S3 shows the aqueous solution system model containing Cu(II) before and after adding the montmorillonite model. The concentration profile curve of Cu(II) in the pure aqueous solution showed a more uniform wavy line with five small peaks at 4–42 Å, suggesting that the Cu(II) ions were uniformly dispersed in the pure aqueous solution. The distribution of Cu(II) showed an ordered monolayer distribution, which was distributed around 0.26 Å above the surface of the montmorillonite layer, indicating that Cu(II) had a strong monolayer adsorption behavior in the montmorillonite interlayer.

3.4.4. Mean square displacement (MSD) and self-diffusion coefficient (D)

The adsorption kinetics study is based on a comparison of the diffusion coefficients of Cu(II) in the pure aqueous phase system and in the aqueous phase system in the presence of montmorillonite to accurately evaluate the adsorption properties of montmorillonite. The MSD of them were computed through the 1,000 ps simulations and the results are presented in Supplementary Figure S4. The diffusion coefficients of Cu(II) in the aqueous phase system and the aqueous solution system containing montmorillonite were $0.13 \times 10^{-8} \mathrm{m}^2 \cdot \mathrm{s}^{-1}$ and $0.85 \times 10^{-10}\ \mathrm{m}^2 \cdot \mathrm{s}^{-1}$, respectively. As expected, the diffusion

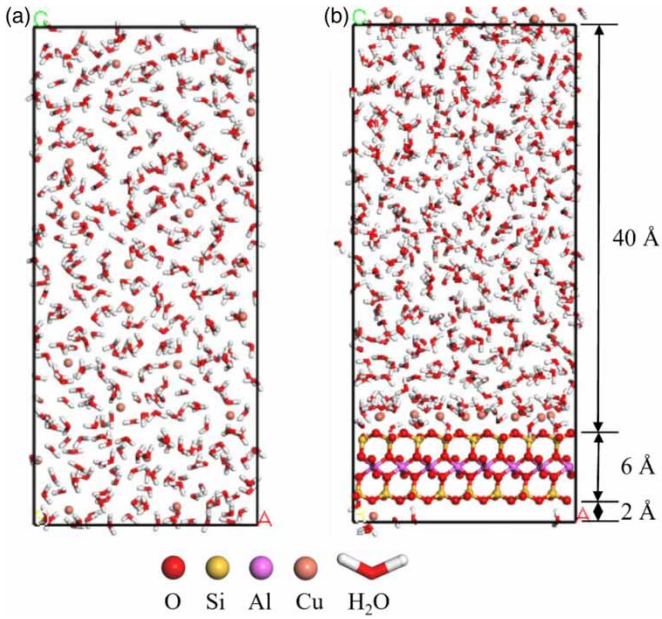

Figure 9 | MD simulation final configuration of Cu(II) in water (a) and MD simulation final configuration of Cu(II) adsorption on the surface of montmorillonite (001) (b).

coefficient of Cu(II) in the aqueous system of montmorillonite was significantly lower than that in the aqueous phase system, indicating strong adsorption of Cu(II) by montmorillonite (Atasoy & Bilgic 2017; Chu *et al.* 2020).

3.4.5. Radial distribution functions

The interaction relationship and microscopic distribution of ions can be deduced by the radial distribution function. The average location of the individual molecules in a solvent is expressed in terms of a radial distribution function, $g(r)$. This function relates the probability of finding another molecule at a particular distance r from each molecule. The interaction between Cu(II) and montmorillonite was studied by using radial distribution function. The radial distribution function results shown in Supplementary Figure S5 are calculated according to the MD simulation trajectory. The first sharp peak was associated with Cu(II) and was located at a distance of 2.25 Å from the surface of the montmorillonite laminate. This indicated that at a distance of 2–3 Å the interaction between Cu(II) and the surface of the montmorillonite laminate is strong and a substantial amount of Cu(II) ions are adsorbed on the surface of the montmorillonite laminate. This is also consistent with the experimental data of SEM-EDS and XRD.

4. CONCLUSION

In this study, the adsorption characteristics and mechanism of Cu(II) on Na-Mt were investigated by means of adsorption experiment and molecular simulation. The characterization of the samples by XRD and EDS showed that Cu(II) was successfully adsorbed on the Na-Mt. The adsorption capacity of Na-Mt on Cu(II) was 35.23 $mg \cdot g^{-1}$ at 80 min. The adsorption process was in accordance with the pseudo-second-order kinetic and the Langmuir isotherm models. The activation energy (E_a) (37.08 $kJ \cdot mol^{-1}$) indicates that the adsorption process was dominated by physical adsorption. The adsorption was a spontaneous, endothermic and entropy-increasing process. The order of influence of coexisting cations on the adsorption capacity of Cu(II) is Mg(II) > Co(II) > Ca(II) > Na(I). The variation in pH has a greater effect on the adsorption capacity of Cu(II) by Na-Mt. After five cycles, Na-Mt still exhibited a high Cu(II) RR of 67%. The simulations demonstrated that there were no significant differences in the adsorption energy of Cu(II) at the four adsorption sites on the surface of montmorillonite(001). The Hirshfeld population analysis found that the electrostatic attraction between Cu(II) and montmorillonite laminate may be stronger compared with Na(I). The diffusion coefficients of Cu(II) in the aqueous phase system and the aqueous solution system containing montmorillonite were 0.13×10^{-8} and $0.85 \times 10^{-10} \cdot m^2 s^{-1}$, respectively. A considerable amount of Cu(II) ions were adsorbed at a distance of 0.26 and 2.25 Å

from the surface of the montmorillonite laminate. These results and methods are important guidelines for the research and application of Cu(II) adsorbents.

ACKNOWLEDGEMENTS

The works were supported by the Major Science and Technology Project of Xinjiang Bingtuan (2020AA004), the Major Science and Technology Project of Bashi Shihezi City (2020ZD02), the National Natural Science Foundation of China (NSFC Grant No. 21968029), the Major Science and Technology Project of Xinjiang Bingtuan (2017AA007), the Applied Basic Research Program of Xinjiang Bingtuan (2015AG004) and Science & Technology Research and Achievement Transformation Project of Xinjiang Bingtuan (2015AD027).

DATA AVAILABILITY STATEMENT

All relevant data are included in the paper or its Supplementary Information.

CONFLICT OF INTEREST

The authors declare there is no conflict.

REFERENCES

Abdullah, W. N. A. S., Tiandee, S., Lau, W., Aziz, F. & Ismail, A. F. 2020 Potential use of nanofiltration like-forward osmosis membranes for copper ion removal. *Chinese Journal of Chemical Engineering* **28** (2), 420–428.

Adapa, S. & Malani, A. 2018 Role of hydration energy and co-ions association on monovalent and divalent cations adsorption at mica-aqueous interface. *Scientific Reports* **8** (1), 12198.

Ameh, T. & Sayes, C. M. 2019 The potential exposure and hazards of copper nanoparticles: a review. *Environmental Toxicology and Pharmacology* **71**, 103220.

Antuganova, Y. O., Sinyakova, M. A., Karmanova, L. A. & Anufrikov, Y. A. 2016 Kinetics of copper and cobalt ion exchange on inorganic antimony-containing ion exchangers. *Russian Journal of Inorganic Chemistry* **61** (12), 1624–1628.

Atasoy, A. D. & Bilgic, B. 2017 Adsorption of copper and zinc ions from aqueous solutions using montmorillonite and bauxite as low-cost adsorbents. *Mine Water and the Environment* **37** (1), 205–210.

Azizian, S. 2004 Kinetic models of sorption: a theoretical analysis. *Journal of Colloid and Interface Science* **276** (1), 47–52.

Behera, U. S., Mishra, P. C. & Radhika, G. B. 2021 Optimization of multiple parameters for adsorption of arsenic (III) from aqueous solution using *Psidium guajava* leaf powder. *Water Science and Technology* **85** (1), 515–534.

Chen, S., Yue, Q., Gao, B., Li, Q., Xu, X. & Fu, K. 2012 Adsorption of hexavalent chromium from aqueous solution by modified corn stalk: a fixed-bed column study. *Bioresource Technology* **113**, 114–120.

Chen, C., Liu, H., Chen, T., Chen, D. & Frost, R. L. 2015 An insight into the removal of Pb(II), Cu(II), Co(II), Cd(II), Zn(II), Ag(I), Hg(I), Cr(VI) by Na(I)-montmorillonite and Ca(II)-montmorillonite. *Applied Clay Science* **118**, 239–247.

Chen, Y., Tang, J., Wang, S. & Zhang, L. 2021a High selectivity and reusability of coordination polymer adsorbents: synthesis, adsorption properties and activation energy. *Microporous and Mesoporous Materials* **324**, 111309.

Chen, Y., Tang, J., Wang, S., Zhang, L. & Sun, W. 2021b Bimetallic coordination polymer for highly selective removal of Pb(II): activation energy, isosteric heat of adsorption and adsorption mechanism. *Chemical Engineering Journal* **425**, 131474.

Chu, Y., Khan, M. A., Zhu, S., Xia, M., Lei, W., Wang, F. & Xu, Y. 2019 Microstructural modification of organo-montmorillonite with Gemini surfactant containing four ammonium cations: molecular dynamics (MD) simulations and adsorption capacity for copper ions. *Journal of Chemical Technology & Biotechnology* **94** (11), 3585–3594.

Chu, Y., Khan, M. A., Xia, M., Lei, W., Wang, F., Zhu, S. & Yan, X. 2020 Synthesis and micro-mechanistic studies of histidine modified montmorillonite for lead(II) and copper(II) adsorption from wastewater. *Chemical Engineering Research and Design* **157**, 142–152.

de Carvalho, D. F., da Fonseca, B. G., Barbosa, I. L., Landi, S. M., de Sena, L. Á., Archanjo, B. S. & Sant'Ana, A. C. 2013 Surface-enhanced Raman scattering study of the redox adsorption of p-phenylenediamine on gold or copper surfaces. *Spectrochimica Acta Part A: Molecular and Biomolecular Spectroscopy* **103**, 108–113.

Douven, S., Paez, C. A. & Gommes, C. J. 2015 The range of validity of sorption kinetic models. *Journal of Colloid and Interface Science* **448**, 437–450.

Fedje, K. K. & Strömvall, A.-M. 2019 Enhanced soil washing with copper recovery using chemical precipitation. *Journal of Environmental Management* **236**, 68–74.

Giusto, L. A. R. & Pissetti, F. L. 2021 Polydimethylsiloxane amino functionalized sponge for adsorption of copper in water. *Journal of Sol-Gel Science and Technology* **99** (1), 243–251.

Greathouse, J. A. & Cygan, R. T. 2005 Molecular dynamics simulation of uranyl(VI) adsorption equilibria onto an external montmorillonite surface. *Physical Chemistry Chemical Physics* **7** (20), 3580–3586.

Grimme, S. 2006 Semiempirical GGA-type density functional constructed with a long-range dispersion correction. *Journal of Computational Chemistry* **27** (15), 1787–1799.

Groenendijk, D. J. & van Wunnik, J. N. M. 2021 Surfactant adsorption and ion exchange on calcite surfaces. *Energy & Fuels* **35** (10), 8763–8772.

Hamid, M. F., Abdullah, N., Yusof, N., Ismail, N. M., Ismail, A. F., Salleh, W. N. W., Jaafar, J., Aziz, F. & Lau, W. J. 2020 Effects of surface charge of thin-film composite membrane on copper (II) ion removal by using nanofiltration and forward osmosis process. *Journal of Water Process Engineering* **33**, 101032.

Han, G., Gu, D., Lin, G., Cui, Q. & Wang, H. 2018 Recovery of lithium from a synthetic solution using spodumene leach residue. *Hydrometallurgy* **177**, 109–115.

Kong, X.-P. & Wang, J. 2016 Copper(II) adsorption on the kaolinite(001) surface: insights from first-principles calculations and molecular dynamics simulations. *Applied Surface Science* **389**, 316–323.

Lima, E. C., Hosseini-Bandegharaei, A., Moreno-Piraján, J. C. & Anastopoulos, I. 2019 A critical review of the estimation of the thermodynamic parameters on adsorption equilibria. Wrong use of equilibrium constant in the Van't Hoof equation for calculation of thermodynamic parameters of adsorption. *Journal of Molecular Liquids* **273**, 425–434.

Liu, J., Xue, W., Bao, Y. & Cheng, W. 2018 Adsorption mechanism of composite whisker on copper ions and lead ions. *Chemical Research in Chinese Universities* **34** (5), 792–797.

Liu, L., Zhang, C., Jiang, W., Li, X., Dai, Y. & Jia, H. 2021 Understanding the sorption behaviors of heavy metal ions in the interlayer and nanopore of montmorillonite: a molecular dynamics study. *Journal of Hazardous Materials* **416**, 125976.

Marcus, Y. 1993 Thermodynamics of solvation of ions. Part 6–The standard partial molar volumes of aqueous ions at 298.15 K. *Journal of the Chemical Society, Faraday Transactions* **89** (4), 713–718.

Maskawat Marjub, M., Rahman, N., Dafader, N. C., Sultana Tuhen, F., Sultana, S. & Tasneem Ahmed, F. 2019 Acrylic acid-chitosan blend hydrogel: a novel polymer adsorbent for adsorption of lead(II) and copper(II) ions from wastewater. *Journal of Polymer Engineering* **39** (10), 883–891.

Molaei, A., Kökkılıç, O. & Waters, K. E. 2018 Selective removal of copper and nickel ions from synthetic process water using predispersed solvent extraction. *The Canadian Journal of Chemical Engineering* **97** (1), 247–255.

Paksamut, J. & Boonsong, P. 2018 Removal of copper(II) ions in aqueous solutions using tannin-rich plants as natural bio-adsorbents. *IOP Conference Series: Materials Science and Engineering* **317**, 012058.

Peng, C., Zhong, Y. & Min, F. 2018 Adsorption of alkylamine cations on montmorillonite (001) surface: a density functional theory study. *Applied Clay Science* **152**, 249–258.

Perdew, J. P., Burke, K. & Ernzerhof, M. 1996 Generalized gradient approximation made simple. *Physical Review Letters* **77** (18), 3865–3868.

Pesavento, M., Profumo, A., Merli, D., Cucca, L., Zeni, L. & Cennamo, N. 2019 An optical fiber chemical sensor for the detection of copper(II) in drinking water. *Sensors* **19** (23), 5246.

Schmidt, R., Bandas, C. D., Gewirth, A. A. & Knaup, J. M. 2021 The adsorption structure of polyethylene imine on copper surfaces for electrodeposition. *Physica Status Solidi (RRL) – Rapid Research Letters* **15** (11), 2100351.

Sharma, A. K., Priya, Kaith, B. S., Singh, A., Isha, Vipula & Chandel, K. 2020 Enzymatic construction of quinine derivative of dextrin/PVA based hybrid gel film for the simultaneous detection and removal of copper and lead ions in real water samples. *Chemical Engineering Journal* **382**.

Szewczuk-Karpisz, K., Tomczyk, A., Komaniecka, I., Choma, A., Adamczuk, A. & Sofinska-Chmiel, W. 2021 Impact of *Sinorhizobium meliloti* exopolysaccharide on adsorption and aggregation in the copper(II) ions/supporting electrolyte/kaolinite system. *Materials (Basel)* **14** (8), 1950.

Tran, H. N. 2022 Improper estimation of thermodynamic parameters in adsorption studies with distribution coefficient K_D (q_e/C_e) or Freundlich constant (K_F): considerations from the derivation of dimensionless thermodynamic equilibrium constant and suggestions. *Adsorption Science & Technology* **2022**, 5553212.

Tran, H. N., Lima, E. C., Juang, R.-S., Bollinger, J.-C. & Chao, H.-P. 2021 Thermodynamic parameters of liquid-phase adsorption process calculated from different equilibrium constants related to adsorption isotherms: a comparison study. *Journal of Environmental Chemical Engineering* **9** (6), 106674.

Tseng, R.-L., Tran, H. N. & Juang, R.-S. 2022 Revisiting temperature effect on the kinetics of liquid–phase adsorption by the Elovich equation: a simple tool for checking data reliability. *Journal of the Taiwan Institute of Chemical Engineers* **136**, 104403.

Turan, N. G. & Ozgonenel, O. 2013 Study of montmorillonite clay for the removal of copper (II) by adsorption: full factorial design approach and cascade forward neural network. *The Scientific World Journal* **2013**, 342628.

Ucarli, O., Yayintas, O. T., Engin, M. S., Cay, S., Saglikoglu, G. & Yilmaz, S. 2020 Investigation of competitive and noncompetitive adsorption of some heavy metals ions on *Leucodon sciuroides* (Hedw.) Schwägr. *Langmuir* **36** (28), 8265–8271.

Unuabonah, E. I., Olu-Owolabi, B. I. & Adebowale, K. O. 2016 Competitive adsorption of metal ions onto goethite–humic acid-modified kaolinite clay. *International Journal of Environmental Science and Technology* **13** (4), 1043–1054.

Vezentsev, A. I., Gorbunova, N. M., Sokolovskiy, P. V., Mar'inskikh, S. G., Chub, A. V., Chau, N. H. & Greish, A. A. 2022 On the adsorption mechanism of copper ions on bentonite clay. *Russian Chemical Bulletin* **71** (4), 651–655.

Viani, A., Gualtieri, A. F. & Artioli, G. 2002 The nature of disorder in montmorillonite by simulation of X-ray powder patterns. *American Mineralogist* **87** (7), 966–975.

Xiao, F., Yan, B.-Q., Zou, X.-Y., Cao, X.-Q., Dong, L., Lyu, X.-J., Li, L., Qiu, J., Chen, P., Hu, S.-G. & Zhang, Q.-J. 2020 Study on ionic liquid modified montmorillonite and molecular dynamics simulation. *Colloids and Surfaces A: Physicochemical and Engineering Aspects* **587**, 124311.

Xing, X., Lv, G., Zhu, W., He, C., Liao, L., Mei, L., Li, Z. & Li, G. 2015 The binding energy between the interlayer cations and montmorillonite layers and its influence on Pb^{2+} adsorption. *Applied Clay Science* **112–113**, 117–122.

Xue, Z., Dong, L., Zhong, Z., Lai, X. & Huang, Y. 2021 Capture effect of Pb, Zn, Cd and Cr by intercalation-exfoliation modified montmorillonite during coal combustion. *Fuel* **290**, 119980.

Yousefzadeh, H., Bozbag, S. E. & Erkey, C. 2022 Supercritical ion exchange: a new method to synthesize copper exchanged zeolites. *The Journal of Supercritical Fluids* **179**, 105417.

Zhao, J. & He, M.-C. 2014 Theoretical study of heavy metal Cd, Cu, Hg, and Ni(II) adsorption on the kaolinite(001) surface. *Applied Surface Science* **317**, 718–723.

Zhou, X. Y., Xue, X. X., Zhao, Y. H. & Liu, O. 2012 Study on adsorption of heavy metal ion in metallurgical wastewater by montmorillonite. *Advanced Materials Research* **461**, 601–605.

Zhu, S., Xia, M., Chu, Y., Khan, M. A., Lei, W., Wang, F., Muhmood, T. & Wang, A. 2019 Adsorption and desorption of Pb(II) on L-lysine modified montmorillonite and the simulation of interlayer structure. *Applied Clay Science* **169**, 40–47.

First received 13 August 2022; accepted in revised form 30 January 2023. Available online 13 February 2023